JACS
JOURNAL OF THE AMERICAN CHEMICAL SOCIETY
Article
pubs.acs.org/JACS

Efficient and Stable Photo-Oxidation of Water by a Bismuth Vanadate Photoanode Coupled with an Iron Oxyhydroxide Oxygen Evolution Catalyst

Jason A. Seabold and Kyoung-Shin Choi*

Department of Chemistry, Purdue University, West Lafayette, Indiana 47907, United States

Supporting Information

ABSTRACT: $BiVO_4$ films were prepared by a simple electrodeposition and annealing procedure and studied as oxygen evolving photoanodes for application in a water splitting photoelectrochemical cell. The resulting $BiVO_4$ electrodes maintained considerable photocurrent for photo-oxidation of sulfite, but generated significantly reduced photocurrent for photo-oxidation of water to oxygen, also decaying over time, suggesting that the photoelectrochemical performance of $BiVO_4$ for water oxidation is mainly limited by its poor catalytic ablity to oxidize water. In order to improve the water oxidation kinetics of the $BiVO_4$ electrode, a layer of FeOOH was placed on the $BiVO_4$ surface as an oxygen evolution catalyst using a new photodeposition route. The resulting $BiVO_4$/FeOOH photoanode exhibitied significantly improved photocurrent and stability for photo-oxidation of water, which is one of the best among all oxide-based phoatoanode systems reported to date. In particular, the $BiVO_4$/FeOOH photoanode showed an outstanding performance in the low bias region (i.e., $E < 0.8$ V vs RHE), which is critical in determining the overall operating current density when assembling a complete p-n photoelectrochemical diode cell. The photocurrent-to-O_2 conversion efficiency of the $BiVO_4$/FeOOH photoanode is ca. 96%, confirming that the photogenerated holes in the $BiVO_4$/FeOOH photoanode are indeed excusively used for O_2 evolution.

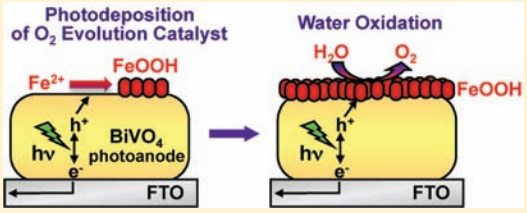

INTRODUCTION

Developement of efficient and practical semiconductor electrodes (photoelectrodes) for use in a water splitting photoelectrochemical cell involves simultaneously satisfying multiple requirements, which remains a challenge. The photoelectrode must absorb visible light, preferably with a direct bandgap transition, and then efficiently separate and utilize the photogenerated carriers to drive desired reactions.[1,2] The multielectron transfers associated with H_2 and O_2 evolution are particularly demanding, thus necessitating surface modification with effective catalysts.[2,3] The semiconductor and its associated catalyst should be composed of inexpensive and abundant elements and should remain stable both chemically and photochemically.[2,4,5] In addition, it is important to develop simple and low-cost methods for electrode preparation and catalyst modification.[1,2] It is also desirable to avoid caustic operating environments and operate in a neutral medium.

Since a single material is unlikely to possess both the narrow bandgap and proper band positions required for efficient water splitting, one prospective solution is known as a p-n photochemical diode.[6−8] In this tandem configuration, which combines an n-type semiconductor (photoanode) and a p-type semiconductor (photocathode), only the holes from the photoanode and the electrons from the photocathode are used for water splitting, while unused carriers from each electrode recombine with one another. As a result, only the valence band edge position of the photoanode and the conduction band edge position of the photocathode are critical concerns. This significantly relaxes the bandgap and band position requirements, broadening the types of materials with a bandgap energy in the visible region that can be used for solar water splitting.

To date, most studies on the development and understanding of semicondutor electrodes for use in a photoelectrochemical cell for water splitting have been performed using simple binary systems (e.g., binary oxides and chalcogenides). However, there are a far greater number of ternary systems that are potentially excellent photoelectrodes but have not been extensively studied. The ternary systems can also offer more possibilities for band gap and band position tuning.[1,9,10] One promising photoanode material is bismuth vanadate ($BiVO_4$), an n-type semiconductor with a direct bandgap of 2.4 eV and the appropriate valence band position for O_2 evolution.[10−13] Its conduction band edge position and flat band potential are fairly negative compared with most other narrow bandgap (i.e., $E_g < 2.6$ eV) oxide-based photoanode materials, located just short of the thermodynamic level for H_2.[10,14] As a result, complete water splitting with $BiVO_4$ requires only a small amount of external bias. In addition, $BiVO_4$ photoanodes do not require the use of strongly acidic or basic media to achieve an optimum photoelectrochemical performance.

In this work, we report a new electrodeposition route to produce amorphous Bi−V−O precursor thin films that can be converted to crystalline n-type $BiVO_4$ electrodes by a mild annealing step. Electrodeposition has the distinctive advantages of being simple, low cost, and easily scalable while enabling

Received: September 24, 2011
Published: January 20, 2012

   dx.doi.org/10.1021/ja209001d | J. Am. Chem.Soc. 2012, 134, 2186−2192

deposition of the material of interest only on the conductive substrate and not on the chamber wall. Previously, synthesis of $BiVO_4$ powders or films has been achieved by chemical bath deposition,[15,16] precipitation,[13] hydrothermal,[17] spray pyrolysis,[18] metal–organic decomposition,[19−22] and the electrochemical oxidation of a bismuth metal layer in the presence of V(V).[23] We also investigated the coupling of $BiVO_4$ electrodes with an iron oxyhydroxide (FeOOH) catalyst layer using a novel yet simple photodeposition method, which significantly improved the O_2 evolution kinetics. The resulting $BiVO_4$/FeOOH electrode generated the highest water splitting photocurrent among $BiVO_4$-based photoanode systems known to date under AM 1.5G illumination (100 mW/cm^2), while also displaying significantly improved stability. In addition, while operating in neutral media (pH = 7), the $BiVO_4$/FeOOH electrode exhibited one of the best performances in the low bias region (<0.8 V vs RHE) compared to other promising oxide-based photoanode systems. The synthesis and characterization of the $BiVO_4$/FeOOH electrodes and the effect of the FeOOH layer on the photoelectrochemical performance and the photostability of the $BiVO_4$ photoanode are discussed in detail.

EXPERIMENTAL SECTION

Materials. Bismuth(III) nitrate ($Bi(NO_3)_3{\cdot}5H_2O$, ≥98.0%) and vanadium(IV) oxide sulfate ($VOSO_4{\cdot}xH_2O$, 97%) were purchased from Sigma Aldrich. Nitric acid (HNO_3, 68.0−70.0%), potassium hydroxide (KOH, pellets), sodium acetate (CH_3COONa, >99.0%), and sodium sulfite (Na_2SO_3, >98.0%) were obtained from Mallinckrodt. Iron(II) chloride ($FeCl_2{\cdot}4H_2O$, 99%) and potassium phosphate monobasic (KH_2PO_4, ACS grade) were from Alfa Aesar and Fisher, respectively. All were used as purchased. Solutions were prepared using high purity water (Millipore Milli-Q purification system, resistivity >18 MΩ·cm).

Glass slides coated with fluorine-doped tin oxide (FTO) were purchased from Hartford Glass, Incorporated. Platinum counter electrodes consisted of a glass slide with a 100 nm electron beam evaporated platinum layer on a 30 nm titanium adhesion layer.

Synthesis of $BiVO_4$ Electrodes. The $BiVO_4$ electrodes used in this study were prepared using an electrodeposition procedure newly developed in this lab. Solutions for electrodeposition were prepared by dissolving 10 mM $Bi(NO_3)_3$ in a solution of 35 mM $VOSO_4$ at < pH 0.5 with HNO_3. Then 2 M sodium acetate was added, raising the pH to ∼5.1, which was then adjusted as needed to pH 4.7 with a few drops of concentrated HNO_3. Acetate serves to stabilize otherwise insoluble Bi(III) ions at pH 4.7. This mildly acidic pH condition must be used, because at pH values where Bi(III) is soluble (<pH 2) no film can be formed, and at pH values above pH 5, V(IV) precipitates from solution. A standard three-electrode cell was used for electrodeposition, with an FTO working electrode, a Ag/AgCl (4 M KCl) reference, and a platinum counter electrode. A Princeton Applied Research VMP2 multichannel potentiostat was used for electrodeposition and all subsequent electrochemical studies. Deposition of amorphous Bi−V−O films was carried out potentiostatically at 1.9 V vs Ag/AgCl for 5 min at 70 °C (ca. 2 mA/cm^2). All freshly prepared films were rinsed and then annealed at 500 °C for 1 h in air, with a 2 °C per minute ramping rate. After annealing, the as-deposited film was converted to crystalline $BiVO_4$ and amorphous V_2O_5, and pure $BiVO_4$ was obtained by dissolving the V_2O_5 in 1 M KOH under stirring for 20 min.

Photodeposition of FeOOH. A layer of FeOOH was conformally photodeposited on the 2 cm^2 $BiVO_4$ films in a 0.1 M $FeCl_2$ solution (pH = 4.1) while stirring. A 300 W Xe arc lamp was used as the light source and the light passed through AM 1.5G and neutral density filters. The intensity of the light that reached the surface of the $BiVO_4$ films was 1.6 mW/cm^2. The photodeposition is based on utilizing photogenerated holes in $BiVO_4$ to oxidize Fe(II) ions to Fe(III) ions that precipitate out as FeOOH on the $BiVO_4$ film (An energy diagram is shown in Supporting Information, Figure S1). Under short circuit conditions with no externally applied bias, however, the photooxidation of Fe(II) ions does not occur readily, as the photoexcited electrons in the conduction band of $BiVO_4$ do not have sufficient potential to reduce water. (Since the solution used for photodeposition was not deaerated, the photoexcited electrons could possibly be used to reduce O_2 under short circuit condition, but the short-circuit photocurrent observed was negligible.) Therefore, in order to facilitate the photooxidation of FeOOH onto $BiVO_4$, a three-electrode cell composed of a $BiVO_4$ working electrode, Pt counter electrode, and Ag/AgCl (4 M KCl) reference electrode was set up, and an external bias was applied in the form of current pulses alternating between 10 μA/cm^2 for 3 s (deposition pulse) and 1 μA/cm^2 for 2 s (resting pulse). The potential required to maintain the deposition current was typically less than 0.2 V vs Ag/AgCl. A typical photodeposition time to deposit an optimum thickness of FeOOH was 5.5 h. The amount of FeOOH deposited on $BiVO_4$ is estimated to be ca. 110 mg/cm^2 based on the photocurrent generated during photodeposition assuming 100% Faradaic efficiency. Since O_2 evolution occurs simultaneously during the photodeposition of FeOOH, the value reported here corresponds to the upper limit of the amount of FeOOH deposited.

Characterization. X-ray diffraction (XRD) was carried out using a Scintag X2 diffractometer (Cu K_α radiation) to confirm the purity and crystallinity of the prepared $BiVO_4$ electrodes. The morphologies of the samples were examined by Scanning Electron Microscopy using an FEI Nova NanoSEM 200 at an accelerating voltage of 5 kV. The SEM samples were first sputter coated with ca. 2 nm thick Pt. Elemental compositions were determined by Energy Dispersive X-ray Spectroscopy (EDX) using the EDX detector on the FEI Nova NanoSEM 200, operated at 20 kV. UV−vis spectra were recorded using a Cary 300 UV−vis spectrophotometer in diffuse reflectance mode. Samples were prepared by scraping the films from the FTO substrate and grinding them with a mortar and pestle before being dispersed over the compact $BaSO_4$ matrix that was used as the reference. When UV−vis spectra were obtained using transmission mode, the thin film morphology generated artificial absorption features (i.e., due to thin film interference and reflection on the surface) that are not truly due to the absorption by $BiVO_4$. X-ray photoelectron spectra (XPS) were obtained using a Kratos Ultra DLD spectrometer using Al K_α radiation (1486.58 eV). The spectra were collected at a fixed analyzer pass energy of 20 eV, and all spectra were calibrated to C 1*s* = 284.6 eV.

Photoelectrochemical and Electrochemical Measurements. Photocurrent measurements utilized simulated solar illumination obtained by passing light from a 300 W Xe arc lamp through neutral density filters and an AM 1.5G filter into an optical fiber and calibrating the output to 100 mW/cm^2 using a thermopile detector from International Light. All samples were back-illuminated through the FTO glass because back-illumination resulted in a much higher photocurrent generation, which is often observed for photoelectrodes with poor electrical conductivity.[22] Back-illumination also allowed for comparing photocurrents generated by $BiVO_4$ and $BiVO_4$/FeOOH electrodes by eliminating the possibility that the FeOOH layer could partially block the photon absorption of the $BiVO_4$ electrode. The illuminated area was either 0.1 or 0.2 cm^2 for all experiments. All photocurrent experiments were conducted in a 0.1 M potassium phosphate buffer at pH 7, using the same three-electrode setup detailed above. In some experiments 0.1 M Na_2SO_3 was added to the electrolyte to compare the photocurrent obtained from sulfite oxidation with the photocurrent obtained from the kinetically more difficult water oxidation reaction. Photocurrents were measured either while sweeping the potential to the positive direction with a scan rate of 10 mV/s or while applying a constant bias under AM 1.5G illumination (100 mW/cm^2). While all measurements were carried out using Ag/AgCl (4 M KCl) reference electrode, results in this study were presented against the reversible hydrogen electrode (RHE) for ease of comparison with the H_2 and O_2 redox levels and with other literature reports that used electrolytes with different pH

dx.doi.org/10.1021/ja209001d | J. Am. Chem.Soc. 2012, 134, 2186−2192

conditions after converting the potential using the following equation.

$$E(\text{vs RHE}) = E(\text{vs Ag/AgCl}) + E_{\text{Ag/AgCl}}(\text{ref}) + 0.0591\text{V} \times \text{pH}$$

$$(E_{\text{Ag/AgCl}}(\text{ref}) = 0.1976\text{V vs NHE at } 25^\circ\text{C})$$

Incident photon-to-current efficiency (IPCE) was determined using illumination from a 150 W Xe arc lamp passed through an AM 1.5G filter and neutral density filters to approximate the output of the sun. Monochromatic light was produced by an Oriel Cornerstone 130 monochromator with a 10 nm bandpass, and the output was measured with a photodiode detector. IPCE was measured in 0.1 M phosphate at pH 7 with the same three-electrode setup described above for photocurrent, using a Princeton Applied Research Potentiostat/Galvanostat model 263A to apply 1.2 V vs RHE.

Capacitance was measured to obtain Mott–Schottky plots for $BiVO_4$ electrodes using a Princeton Applied Research Potentiostat/Galvanostat model 263A connected to a Princeton Applied Research FRD100 frequency response detector. A sinusoidal modulation of 10 mV was applied at frequencies of 5 kHz and 10 kHz. The three-electrode setup was used with a 0.1 M phosphate buffer at pH 7.

Oxygen Detection. Oxygen was detected quantitatively using an Ocean Optics fluorescence-based oxygen sensor (FOSPOR-R 1/16"). The electrochemical cell was a custom-built airtight two-compartment cell divided by a frit. One side held a Pt counter electrode, while the other side held the working electrode ($BiVO_4$/FeOOH) along with a Ag/AgCl reference electrode. Both sides were filled with 0.1 M KH_2PO_4 and degassed with argon. The electrolyte in the working compartment was 22.4 mL and the headspace volume was 15.2 mL. The needle probe was inserted through a rubber septum and made continuous O_2 readings at 1 s intervals throughout the experiment. The probe was calibrated using 2 points (argon, 0% O_2, and air, 20.9% O_2), with an error of 5% of the reading. The experiment began with 30 min of baseline O_2 measurement followed by 2 h of illumination using light passed through an AM 1.5G filter and adjusted to 200 mW/cm^2 (2 suns) and 0.5 V applied bias. The use of an intense light (200 mW/cm^2) for the O_2 detection experiment was to ensure a higher signal-to-noise ratio and therefore more reliable data. The probe measures the O_2 content in the headspace and records as mole %. This was converted to μmol after first adjusting for the O_2 dissolved in solution using Henry's Law. See Supporting Information for more details regarding O_2 detection experiments.

RESULTS AND DISCUSSION

The bismuth vanadate films were anodically electrodeposited using an aqueous solution containing Bi(III) ions and V(IV) ions (pH 4.7). Upon application of 1.9 V vs Ag/AgCl, V(IV) ions were oxidized to V(V) ions and precipitated out with Bi(III) ions to form a brownish gray film on the FTO working electrode. The as-deposited film was X-ray amorphous but an XPS study confirmed that it contained Bi(III) and V(V) ions (Supporting Information, Figure S2).[23,24] However, it did not appear to be $BiVO_4$ judging from its color, as $BiVO_4$ is bright yellow. In addition, the as-deposited film dissolved readily in 1 M KOH while $BiVO_4$ is reported to be stable in basic media. EDX analysis of the as-deposited films indicated a Bi:V ratio of 2:3. The as-deposited material may be $Bi_4V_6O_{21}$, which is reported to be a stable compound in the Bi–V–O family composed of Bi(III) and V(V) ions with a stoichiometry matching our EDX data.[25,26] Unfortunately, positive identification of the $Bi_4V_6O_{21}$ phase is difficult, as the film is amorphous, and very little Raman or XPS information exists concerning this phase.

The as-deposited film was decomposed into crystalline $BiVO_4$ and amorphous V_2O_5 when annealed in air at 500 °C for 1 h (Figure 1). Although XRD only detected the presence of

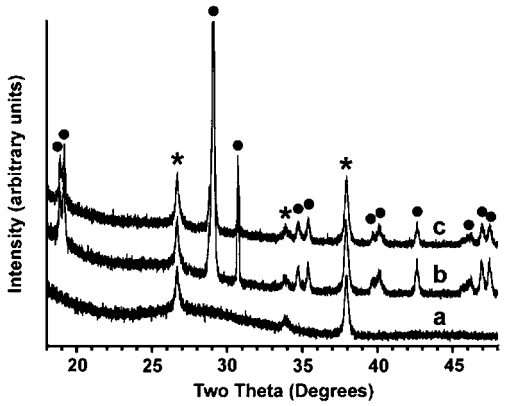

Figure 1. XRD of (a) an as-deposited Bi–V–O film, and annealed films (b) before and (c) after soaking in KOH solution to dissolve V_2O_5 (* = peaks from FTO, ● = peaks from $BiVO_4$).

the crystalline $BiVO_4$ phase, the presence of amorphous V_2O_5 in the annealed sample was inferred since the Bi:V ratio in the as-deposited film was 2:3, which results in excess vanadium once the 1:1 $BiVO_4$ phase is formed. The red hue of the annealed film was a strong indication of the presence of V_2O_5 since a pure $BiVO_4$ film would appear yellow. This red hue disappeared when the film was immersed in 1 M KOH for 20 min where V_2O_5 is soluble, resulting in a uniform yellow film. EDX confirmed that the dissolution process changed the Bi:V ratio from 2:3 to 1:1. XRD of the film after the dissolution process showed that the crystalline peaks of $BiVO_4$ remained intact (Figure 1). A UV–vis spectrum of the $BiVO_4$ film was obtained using diffuse reflectance method and its bandgap was estimated to be 2.4 eV, which agrees well with values for the bandgap energy of $BiVO_4$ reported in the literature. (Supporting Information, Figure S3).[10–12,21,22]

SEM images of an as-deposited film and an annealed film before and after the removal of V_2O_5 are shown in Figure 2.

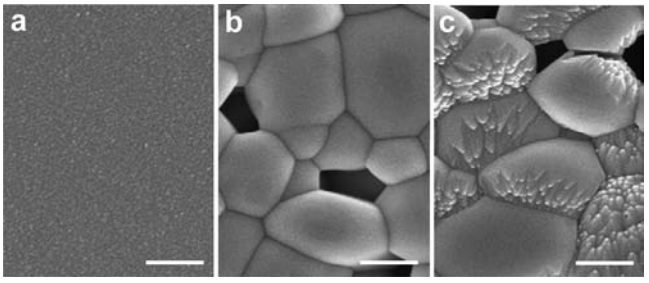

Figure 2. SEM images of (a) an as-deposited Bi–V–O film, and annealed films (b) before and (c) after soaking in KOH solution to dissolve V_2O_5 (scale bar, 250 nm).

The as-deposited film has a smooth and featureless surface (Figure 2a), but the annealed film is composed of adjoining larger grains ranging from 200 to 500 nm (Figure 2b). When the amorphous V_2O_5 phase, which fills in and around the crystalline $BiVO_4$ grains, is dissolved, each $BiVO_4$ grain exhibits a roughened surface (Figure 2c).

LSVs both in the dark and under AM 1.5G 100 mW/cm^2 illumination were performed on a $BiVO_4$ film in 0.1 M phosphate buffer at pH 7 with and without the addition of 0.1 M sodium sulfite (Na_2SO_3). As expected for an n-type semiconductor, the $BiVO_4$ electrode served as a photoanode and generated anodic photocurrent through the consumption

dx.doi.org/10.1021/ja209001d | J. Am. Chem.Soc. 2012, 134, 2186–2192

of photoinduced holes for water oxidation at the semiconductor/electrolyte interface (Figure 3a). When sulfite was

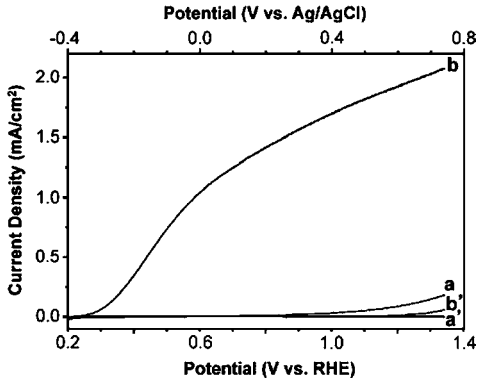

Figure 3. Current–potential characteristics of a $BiVO_4$ photoanode obtained under AM 1.5G illumination (100 mW/cm^2) in (a) 0.1 M KH_2PO_4 and (b) 0.1 M KH_2PO_4 with 0.1 M Na_2SO_3, both at pH 7. a′ and b′ are the corresponding LSVs obtained in the dark (scan rate = 10 mV/s).

added, the anodic photocurrent density increased several times as shown in Figure 3b. This is because in the presence of sulfite, the anodic photocurrent generated is exclusively due to oxidation of sulfite, which is kinetically much easier than water oxidation.[27,28] Thus, the substantial enhancement in photocurrent in the presence of sulfite demonstrates that the water oxidation photocurrent of the $BiVO_4$ electrode is mainly limited by poor kinetics for water oxidation on its surface. In fact, the photocurrent generated by $BiVO_4$ for sulfite oxidation shown in Figure 3 is very exciting in that few oxide-based photoanodes known to date can generate photocurrent at that level in a pH 7 medium. This result suggests that it may be possible for $BiVO_4$ to generate a similar level of photocurrent for water oxidation when it is coupled with a proper oxygen evolution catalyst.

To probe this possibility, we placed a simple, low cost, and practical Fe-based oxygen evolution catalyst, iron oxyhydroxide (FeOOH), on the $BiVO_4$ surface and investigated its effects on the photoanode performance. FeOOH is known to be capable of evolving O_2 at moderate overpotentials,[29−31] but has been less studied than Co and Ni oxides/hydroxides[32,33] and to date, it has not been coupled with a semiconductor for use in the photo-oxidation of water. The most effective way to place OEC on the surface of a photoanode is to use the photo-oxidative reactivity that exists at the illuminated photoanode surface. If valence band holes are used to produce OEC, then the OECs will be selectively deposited at locations where holes are readily generated or available. This allows for placing OEC preferentially at the locations where photo-oxidation of water can most readily occur, thus ensuring their most efficient use.[34−36] Therefore, developing a synthesis method to produce FeOOH utilizing holes from the VB of $BiVO_4$ would be highly advantageous for the purpose of producing efficient $BiVO_4$/FeOOH photoanode systems.

Recently, we reported the anodic electrodeposition of FeOOH via oxidation of Fe(II) ions to Fe(III) ions in an aqueous medium of pH 4.1.[37] As the solubility of Fe(III) in this medium is very limited, precipitation of FeOOH resulted on the working electrode surface. While the resulting film was X-ray amorphous, it was identified by Raman as a γ-FeOOH phase lacking long-range order. γ-FeOOH is reported to have higher activity for water oxidation than α-FeOOH.[38,39] In this study, we probed the possibility of utilizing photogenerated holes from $BiVO_4$ to oxidize Fe(II) ions to Fe(III) ions to form FeOOH on the $BiVO_4$ surface. Since the valence band edge of $BiVO_4$ is located at 2.4 V vs RHE, it is thermodynamically feasible to use valence band holes to oxidize Fe(II) ions.

The photodepositions were carried out on the $BiVO_4$ electrode immersed in 0.1 M $FeCl_2$ (pH 4.1) solution while stirring. Films were back-illuminated through the FTO with an intensity of 1.6 mW/cm^2. To aid the photodeposition, an external bias was applied to generate a deposition current pulse of 10 μA/cm^2 for 3 s followed by a resting current pulse of 1 μA/cm^2 for 2 s, alternating in this manner for a desired period of time. The potential required to maintain the deposition current pulses was typically less than 0.2 V vs Ag/AgCl. In this potential range, there is very little dark current (~1 μA/cm^2), meaning that the electrochemical oxidation of Fe(II) ions is not feasible. Therefore, the 10 μA/cm^2 anodic deposition current under illumination is driven almost entirely by the oxidation of Fe(II) ions via photogenerated holes from the valence band of $BiVO_4$. The role of the applied potential is to create a sufficient band bending at the $BiVO_4$/electrolyte junction to increase the surface hole concentration in order to generate 10 μA/cm^2 of photodeposition current (See the Experimental Section for further explanation of the role of applied potential).

As the amount of FeOOH deposited on the $BiVO_4$ surface increases, O_2 evolution kinetics are improved and the photocurrent due to O_2 evolution is added to the photocurrent due to Fe(II) oxidation. As a result, the same level of photocurrent (i.e., 10 μA/cm^2) can be generated with a successively smaller degree of band bending, and therefore the potential necessary to generate the 10 μA/cm^2 gradually decreases. When the FeOOH reaches an optimum thickness, the potential passes through a minimum and begins to increase. This makes it possible to identify the optimum amount of FeOOH to enhance photocurrent by monitoring the potential necessary to generate 10 μA/cm^2 of current pulses. A typical photodeposition reached an optimum thickness within 5.5 h. Top and cross-sectional view SEM images of an FeOOH layer deposited on the $BiVO_4$ film to maximize the photocurrent output are shown in Figure 4. The FeOOH layer conformally

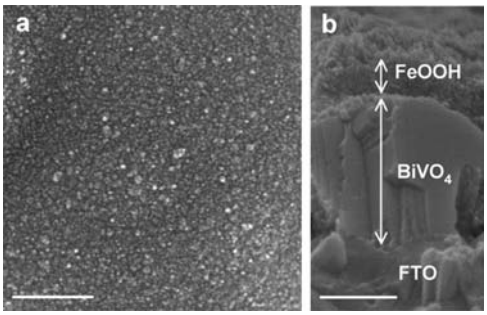

Figure 4. SEM images showing (a) top view and (b) cross-sectional view of a $BiVO_4$/FeOOH photoanode (scale bar, 250 nm).

covers the $BiVO_4$ film and is approximately 150 nm thick. Since the bandgap of FeOOH is ca. 2 eV, the color of the $BiVO_4$/FeOOH film became orange-red (Supporting Information, Figure S3).

LSVs of our best (i.e., top 10% of the samples) and average $BiVO_4$/FeOOH under illumination were obtained in phosphate buffer at pH 7 (Figure 5). The $BiVO_4$/FeOOH films displayed

dx.doi.org/10.1021/ja209001d | J. Am. Chem.Soc. 2012, 134, 2186–2192

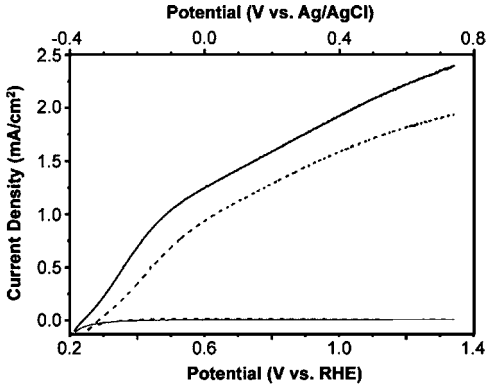

Figure 5. Current–potential characteristics of $BiVO_4$/FeOOH photoanodes obtained in 0.1 M KH_2PO_4 (pH 7) under AM 1.5G illumination (100 mW/cm^2); solid line: top 10% sample, dotted line: average sample, gray lines: dark currents for both cases (scan rate = 10 mV/s).

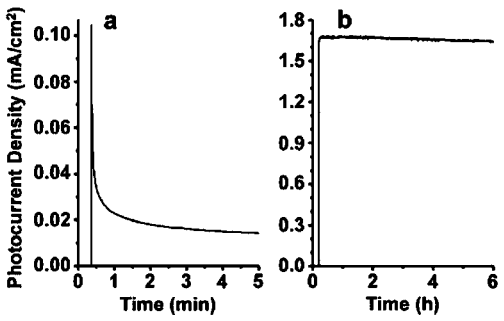

Figure 6. Photocurrent obtained at 1.2 V vs RHE of (a) a bare $BiVO_4$ and (b) a $BiVO_4$/FeOOH photoanode obtained in 0.1 M KH_2PO_4 (pH 7) under AM 1.5G illumination (100 mW/cm^2).

remarkably improved photocurrent, which is comparable to photocurrent generated by bare $BiVO_4$ using sulfite as the hole scavenger (Figure 3b), verifying the ability of FeOOH to efficiently collect photogenerated holes from the $BiVO_4$ layer and facilitate water oxidation to O_2. A comparison of Figures 5 and 3a also shows that when FeOOH is present, the photocurrent onset is shifted in the negative direction by 500 mV toward its flatband potential, which is reported to range from 0.02 V to −0.1 V vs RHE (Supporting Information, Figure S4).[14,19,40] This indicates that the slow kinetics of oxygen evolution on $BiVO_4$ are also responsible for the delayed onset of water oxidation photocurrent by causing severe surface recombination.

The photocurrent of our $BiVO_4$/FeOOH film obtained from water oxidation (with no sacrificial hole acceptors, scan rate = 10 mV/s) is the highest of any known $BiVO_4$-based film to date.[3,14,19−22] In addition, when compared to LSVs of other reported oxide-based photoanode systems (scan rate ≥10 mV/s), the photocurrent generated by the $BiVO_4$/FeOOH electrode in the low bias region (i.e., below 0.8 V against RHE) is particularly outstanding. For example, our best (i.e., top 10% of the samples) and average $BiVO_4$/FeOOH electrodes attain 1.0 mA/cm^2 at a record ca. 0.5 and 0.6 V, respectively, vs RHE, which is a several hundred mV improvement (i.e., a shift to the negative direction) over most oxide-based photoanodes that have shown very promising performances.[14,36,41−44] This characteristic, which results in achieving the maximum power for the water oxidation half reaction at a potential closer to the thermodynamic potential of water reduction, is critical in maximizing the operating current density in a complete p-n photoelectrochemical diode cell (Supporting Information, Figure S5).[2]

The effect of FeOOH on the photostability of $BiVO_4$ was also examined by measuring and comparing photocurrent densities of a bare $BiVO_4$ electrode and a $BiVO_4$/FeOOH electrode in phosphate solution at 1.2 V vs RHE under AM 1.5G illumination (100 mW/cm^2) for 6 h (Figure 6). The photocurrent generated by the bare $BiVO_4$ film decreases significantly within a few minutes, indicating that accumulation of photogenerated holes at the surface of $BiVO_4$ due to poor kinetics for water oxidation results in severe anodic photocorrosion. Photocorrosion or a decay of photocurrent over time have been reported in the literature for $BiVO_4$. Although the detailed mechanism of the photocorrosion has not been described, it is reported that the surface ratio of V/Bi decreases significantly during illumination, resulting in a bismuth rich surface layer and a considerable reduction in photocurrent.[11,20] When the FeOOH layer was added to the surface of the $BiVO_4$ electrode, a photocurrent density of 1.7 mA/cm^2 was maintained for 6 h with only 2% of decay. Photostability of $BiVO_4$-based systems at this high level of photocurrent density for several hours has been rarely achieved since the degree of photocorrosion is generally proportional with the amount of photocurrent generated. This result demonstrates the exceptional promise of FeOOH for improving photostability as well as photocurrent of $BiVO_4$. Perfect coverage of the $BiVO_4$ surface by FeOOH apears to be necessary to completely prevent the photocorrosion, and the observed 2% decay is most likely due to the cracks of the $BiVO_4$ electrodes where photodeposition of FeOOH was not feasible.

$BiVO_4$ photoanodes have been previously combined with various catalysts to enhance the O_2 evolution of $BiVO_4$ while reducing photocorrosion. One attempt was to modify the surface of $BiVO_4$ with Ag(I) ions, which involved simply dipping the $BiVO_4$ electrode in an $AgNO_3$ solution. Although the exact form of the responsible species was not identified, the Ag-modified $BiVO_4$ electrode enhanced O_2 evolution and also noticeably improved the stability, although the corrosion was not fully suppressed.[19] In another study, $BiVO_4$ was coupled with IrO_x, Co_3O_4, and Pt.[3] Pt-modified $BiVO_4$ gave the best photocurrent performance and was the only electrode with enhanced stability. Surprisingly, IrO_x, which is a good electrocatalyst for OER and is used to enhance photocurrent of other semiconductor electrodes, resulted in no enhancement when coupled with $BiVO_4$. This is a good example demonstrating that the performance of an OEC depends significantly on the nature of the semiconductor and the semiconductor/OEC interface. This is because the semiconductor/OEC interface or the OEC itself can significantly affect the generation, separation, and recombination of photoinduced charge carriers in the semiconductor electrode.[45] Two very recent examples are Mo- or W-doped $BiVO_4$ electrodes coupled with Co-Pi OEC, which resulted in the ehancement of both photocurrent and photostability.[21,22] When deposited on a conducting substrate and compared for electrochemical water oxidation, Co-Pi OEC shows a better catalytic performance than FeOOH (Supporting Information, Figure S6). However, when the enhancement of Mo- or W-doped $BiVO_4$ achieved using Co-Pi OEC is compared with that demonstrated in this study using FeOOH, FeOOH appears to

enhance the photocurrent of the $BiVO_4$ electrode more considerably. In addition, when Co-Pi OEC was deposited on our $BiVO_4$ electrode, no evident photocurrent enhancement was observed. These results and comparisons demonstrate that the performance of OEC coupled with a semiconductor can be different from the performance of OEC on a conducting substrate and that even when the same types of semiconductor electrode and OEC are combined, their overall performance can vary significantly depending on the details of the semiconductor/OEC interface.

In order to confirm that the anodic photocurrent produced by the $BiVO_4$/FeOOH electrode is the exclusive result of O_2 evolution, O_2 production and photocurrent were monitored concurrently under 0.5 V (vs RHE) bias using 200 mW/cm^2 AM 1.5G filtered illumination, and the theoretical O_2 production calculated from photocurrent was compared with the actual O_2 yield measured by a fluorescence-based O_2 sensor. This value, the photocurrent-to-oxygen conversion efficiency was 96%, demonstrating the high selectivity of the photo-oxidation reaction occurring on the $BiVO_4$/FeOOH photo-anode (Figure 7). The remaining 4% is most likely associated

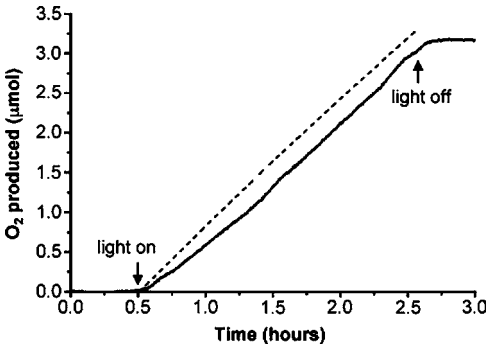

Figure 7. O_2 detected by a fluorescence-based sensor (—), and O_2 calculated from photocurrent assuming 100% faradaic efficiency for O_2 evolution (---) during illumination of a $BiVO_4$/FeOOH photoanode at 0.5 V vs RHE in 0.1 M KH_2PO_4, pH 7 (200 mW/cm^2, AM 1.5G filtered illumination).

with photocorrosion processes, which are enabled by imperfect coverage of the $BiVO_4$ surface by FeOOH as discussed earlier.

IPCE analysis of the $BiVO_4$ films in phosphate buffer at 1.2 V vs RHE shows a substantial improvement when FeOOH is present (Figure 8). Bare $BiVO_4$ reaches a maximum of 9% at

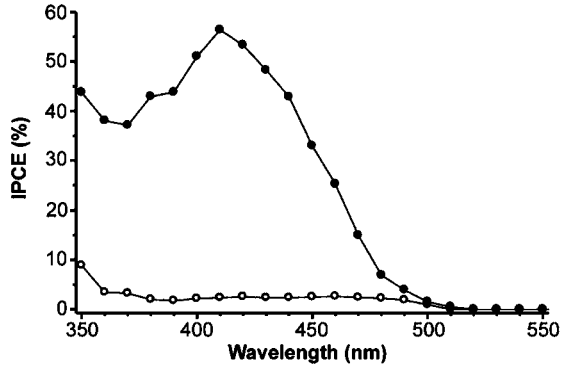

Figure 8. IPCE of bare $BiVO_4$ (open circles) and $BiVO_4$/FeOOH (filled circles) photoanodes obtained at 1.2 V vs RHE in 0.1 M KH_2PO_4 (pH 7).

350 nm, while the $BiVO_4$/FeOOH film achieves 44% at this wavelength, and reaches 56% at 410 nm. The IPCE analysis also shows that the photocurrent response begins at 510 nm, regardless of the presence of FeOOH. This corresponds to 2.43 eV and indicates that although FeOOH itself is a semiconductor with a bandgap of 2 eV, it does not appreciably contribute to the photoactivity of the $BiVO_4$/FeOOH film and mainly performs as a catalyst.[37,46] This observation also agrees well with the fact that the photocurrent obtained by the FeOOH layer alone is negligible (Supporting Information, Figure S7). This is because FeOOH is a poor photon absorber and a poor electrical conductor.[37,46] When the measured IPCE of the $BiVO_4$/FeOOH sample was weighted by the number of photons available at each wavelength under the AM 1.5G spectrum and integrated across all wavelengths,[47] the calculated current was 1.89 mA/cm^2, which agrees well with the photocurrent observed for the average sample at this potential (Figure 5).

The maximum attainable photocurrent for a material with a 2.4 eV bandgap is ~7.6 mA/cm^2 under AM 1.5G solar irradiation.[47] At high applied bias, our $BiVO_4$/FeOOH reaches ~30% of this maximum. The factors limiting further improvements likely include incomplete light absorption by the thin $BiVO_4$ film and recombination losses in the bulk. Making the films thicker increased their absorbance, but reduced their photocurrent, most likely due to bulk carrier recombination. This challenge may be overcome in the future by introducing nanostructure that increases the volume of the space charge layer and shortens the distance that minority carriers must travel, thus greatly enhancing charge separation and the overall efficiency.

■ CONCLUSIONS

$BiVO_4$ photoanodes for use in a photoelectrochemical water splitting cell were prepared by a simple electrodeposition and heat treatment process. The resulting film produced low and unsustainable photocurrent for water oxidation but generated a significant and stable photocurrent for oxidation of sulfite, indicating that its poor performance for photo-oxidation of water was mainly due to the poor catalytic ability of the $BiVO_4$ surface for water oxidation. After coating the $BiVO_4$ surface with a catalytic FeOOH layer via a new photodeposition route, the films were capable of utilizing a substantially greater number of holes which reached the semiconductor/liquid junction for photo-oxidation of water and generated the highest photocurrent among $BiVO_4$-based electrodes reported to date, while attaining significant stability compared to bare $BiVO_4$. In fact, the performance shown by the $BiVO_4$/FeOOH in the $E <$ 0.8 V vs RHE region, reaching 1.0 mA/cm^2 at only ca. 0.5 V vs RHE, is remarkable compared to the performances of other oxide-based photoanode systems known to date. O_2 measurements confirmed that the anodic photocurrent of the $BiVO_4$/FeOOH photoanode is exclusively due to O_2 evolution. The outstanding performance, accomplished using inexpensive semiconductor and catalyst materials produced from facile, practical, and mild synthesis conditions while operating in a neutral medium, suggests that a further study on the $BiVO_4$/FeOOH photoanode system including composition tuning and incorporation of nanostructure can be a very promising avenue to an efficient water-splitting photoanode for use in a photoelectrochemical diode.

dx.doi.org/10.1021/ja209001d | J. Am. Chem.Soc. 2012, 134, 2186–2192

■ ASSOCIATED CONTENT

Supporting Information

UV−vis spectra, XPS spectra, and Mott−Schottky plots of $BiVO_4$ electrodes, LSVs of Co-Pi OEC and FeOOH for electrical water oxidation, photocurrent of FeOOH, a scheme showing band positions of $BiVO_4$ as well as various redox potentials discussed in this study, and a scheme showing the expected maximum operating current density in a complete p-n photoelectrochemical diode. This material is available free of charge via the Internet at http://pubs.acs.org.

■ AUTHOR INFORMATION

Corresponding Author

kchoi1@purdue.edu

■ ACKNOWLEDGMENTS

This work was financially supported by a Center for Chemical Innovation of the National Science Foundation (Grant CHE-0802907) and made use of the Life Science Microscopy Facility at Purdue University.

■ REFERENCES

(1) Osterloh, F. E.; Parkinson, B. A. *MRS Bull.* **2011**, *36*, 17.
(2) Walter, M. G.; Warren, E. L.; McKone, J. R.; Boettcher, S. W.; Mi, Q. X.; Santori, E. A.; Lewis, N. S. *Chem. Rev.* **2010**, *110*, 6446−6473.
(3) Ye, H.; Park, H. S.; Bard, A. J. *J. Phys. Chem. C* **2011**, *115*, 12464−12470.
(4) Chen, Z. B.; Jaramillo, T. F.; Deutsch, T. G.; Kleiman-Shwarsctein, A.; Forman, A. J.; Gaillard, N.; Garland, R.; Takanabe, K.; Heske, C.; Sunkara, M.; McFarland, E. W.; Domen, K.; Miller, E. L.; Turner, J. A.; Dinh, H. N. *J. Mater. Res.* **2010**, *25*, 3−16.
(5) Turner, J.; Sverdrup, G.; Mann, M. K.; Maness, P. C.; Kroposki, B.; Ghirardi, M.; Evans, R. J.; Blake, D. *Int. J. Energ. Res.* **2008**, *32*, 379−407.
(6) Yoneyama, H.; Sakamoto, H.; Tamura, H. *Electrochim. Acta* **1975**, *20*, 341−345.
(7) Nozik, A. J. *Appl. Phys. Lett.* **1976**, *29*, 150−153.
(8) Nozik, A. J. *Appl. Phys. Lett.* **1977**, *30*, 567−569.
(9) Matsumoto, Y. *J. Solid State Chem.* **1996**, *126*, 227−234.
(10) (a) Walsh, A.; Yan, Y.; Huda, M. N.; Al-Jassim, M. M.; Wei, S.-H. *Chem. Mater.* **2009**, *21*, 547−551. (b) Yin, W.-J.; Wei, S.-H.; Al-Jassim, M. M.; Turner, J.; Yan, Y. *Phys. Rev. B* **2011**, *83*, 155102.
(11) Berglund, S. P.; Flaherty, D. W.; Hahn, N. T.; Bard, A. J.; Mullins, C. B. *J. Phys. Chem. C* **2011**, *115*, 3794−3802.
(12) Kudo, A.; Ueda, K.; Kato, H.; Mikami, I. *Catal. Lett.* **1998**, *53*, 229−230.
(13) Iwase, A.; Kudo, A. *J. Mater. Chem.* **2010**, *20*, 7536−7542.
(14) Hong, S. J.; Lee, S.; Jang, J. S.; Lee, J. S. *Energ. Environ. Sci.* **2011**, *4*, 1781−1787.
(15) Su, J. Z.; Guo, L. J.; Yoriya, S.; Grimes, C. A. *Cryst. Growth Des.* **2010**, *10*, 856−861.
(16) Neves, M. C.; Trindade, T. *Thin Solid Films* **2002**, *406*, 93−97.
(17) Yu, J. Q.; Kudo, A. *Chem. Lett.* **2005**, *34*, 850−851.
(18) Dunkle, S. S.; Helmich, R. J.; Suslick, K. S. *J. Phys. Chem. C* **2009**, *113*, 11980−11983.
(19) Sayama, K.; Nomura, A.; Arai, T.; Sugita, T.; Abe, R.; Yanagida, M.; Oi, T.; Iwasaki, Y.; Abe, Y.; Sugihara, H. *J. Phys. Chem. B* **2006**, *110*, 11352−11360.
(20) Sayama, K.; Wang, N. N.; Miseki, Y.; Kusama, H.; Onozawa-Komatsuzaki, N.; Sugihara, H. *Chem. Lett.* **2010**, *39*, 17−19.
(21) Pilli, S. K.; Furtak, T. E.; Brown, L. D.; Deutsch, T. G.; Turner, J. A.; Herring, A. M. *Energy Environ. Sci.* **2011**, *4*, 5028−5034.
(22) Zhong, D. K.; Choi, S.; Gamelin, D. R. *J. Am. Chem. Soc.* **2011**, *133*, 18370−18377.
(23) Myung, N. M., N.; Ham, S.; Choi, S.; Chae, Y.; Kim, W. G.; Jeon, Y. J.; Paeng, K. J.; Chanmanee, W.; de Tacconi, N. R.; Rajeshwar, K. *J. Phys. Chem. C* **2011**, *115*, 7793−7800.
(24) NIST X-ray Photoelectron Spectroscopy Database, Version 3.5; National Institute of Standards and Technology, Gaithersburg, 2003); http://srdata.nist.gov/xps/
(25) Cho, Y. G.; Park, D. K.; Park, D. W.; Woo, H. C.; Chung, J. S. *Res. Chem. Intermed.* **2002**, *28*, 419−431.
(26) Zyryanov, V. V. *Inorg. Mater.* **2005**, *41*, 156−163.
(27) Reber, J. F.; Meier, K. *J. Phys. Chem.* **1984**, *88*, 5903−5913.
(28) Liu, W.; Ye, H. C.; Bard, A. J. *J. Phys. Chem. C* **2010**, *114*, 1201−1207.
(29) Lohrengel, M. M.; Richter, P. K.; Schultze, J. W. *Ber. Bunsen Phys. Chem.* **1979**, *83*, 490−495.
(30) Schultze, J. W.; Mohr, S.; Lohrengel, M. M. *J. Electroanal. Chem.* **1983**, *154*, 57−68.
(31) Lyons, M. E. G.; Burke, L. D. *J. Electroanal. Chem.* **1984**, *170*, 377−381.
(32) Lyons, M. E. G.; Brandon, M. P. *J. Electroanal. Chem.* **2010**, *641*, 119−130.
(33) Lyons, M. E. G.; Brandon, M. P. *Int. J. Electrochem. Sc.* **2008**, *3*, 1463−1503.
(34) Steinmiller, E. M. P.; Choi, K. S. *P. Natl. Acad. Sci. USA* **2009**, *106*, 20633−20636.
(35) McDonald, K. J.; Choi, K. S. *Chem. Mater.* **2011**, *23*, 1686−1693.
(36) Zhong, D. K.; Cornuz, M.; Sivula, K.; Graetzel, M.; Gamelin, D. R. *Energ. Environ. Sci.* **2011**, *4*, 1759−1764.
(37) Spray, R. L.; Choi, K. S. *Chem. Mater.* **2009**, *21*, 3701−3709.
(38) Elizarova, G. L.; Matvienko, L. G.; Kuznetsov, V. L.; Kochubey, D. I.; Parmon, V. N. *J. Mol. Catal. A-Chem.* **1995**, *103*, 43−50.
(39) Elizarova, G. L.; Zhidomirov, G. M.; Parmon, V. N. *Catal. Today* **2000**, *58*, 71−88.
(40) Ye, H. C.; Lee, J.; Jang, J. S.; Bard, A. J. *J. Phys. Chem. C* **2010**, *114*, 13322−13328.
(41) Tilley, S. D.; Cornuz, M.; Sivula, K.; Gratzel, M. *Angew. Chem., Int. Ed.* **2010**, *49*, 6405−6408.
(42) Abe, R.; Higashi, M.; Domen, K. *J. Am. Chem. Soc.* **2010**, *132*, 11828−11829.
(43) Cristino, V.; Caramori, S.; Argazzi, R.; Meda, L.; Marra, G. L.; Bignozzi, C. A. *Langmuir* **2011**, *27*, 7276−7284.
(44) Santato, C.; Ulmann, M.; Augustynski, J. *J. Phys. Chem. B* **2001**, *105*, 936−940.
(45) Seabold, J. A.; Choi, K. S. *Chem. Mater.* **2011**, *23*, 1105−1112.
(46) Cornell, R. M.; Schwertmann, U. *The Iron Oxides: Structure, Properties, Reactions, Occurrences and Uses*; 2nd ed.; Wiley-VCH: New York, 2003.
(47) ASTM Standard G173 - 03, 2008, "Standard Tables for Reference Solar Spectral Irradiances: Direct Normal and Hemispherical on 37° Tilted Surface"; ASTM International: West Conshohocken, PA, 2003, DOI: 10.1520/G0173-03R08, www.astm.org.